Received January 5, 2019, accepted January 29, 2019, date of publication February 4, 2019, date of current version February 22, 2019.

Digital Object Identifier 10.1109/ACCESS.2019.2897361

Curved-Path Sar Geolocation Error Analysis Based On Bp Algorithm

JUNBIN LIU[1,2,3], XIAOLAN QIU[2,3], (Senior Member, IEEE), LIJIA HUANG[2,3], AND CHIBIAO DING[3]

[1]School of Electronic, Electrical and Communication Engineering, University of Chinese Academy of Sciences, Beijing 100049, China
[2]Key Laboratory of Technology in Geo-Spatial Information Processing and Application System, Chinese Academy of Sciences, Beijing 100190, China
[3]Institute of Electronics, Chinese Academy of Sciences, Beijing 100190, China

Corresponding author: Xiaolan Qiu (xlqiu@mail.ie.ac.cn)

This work was supported by the National Nature Science Foundation of China (NSFC) under Grant 61331017.

ABSTRACT The theoretical modeling and analysis of synthetic aperture radar (SAR) location error play an important role in SAR system design and error source budget. The existing SAR geolocation error models are mainly implicit, which are not easy to do analysis, especially in the curved-path case. In this paper, a theoretical explicit model of the relationship between image geolocation error and the path measurement error is established for curved-path SAR, based on back projection imaging algorithm. The simulations of multiple sets of parameters verify the correctness of the proposed model. The explicit model and the analysis results provide an effective reference for understanding and budgeting the system-level geometric location error for curved-path SAR, such as geosynchronous orbit synthetic aperture radar.

INDEX TERMS BP imaging, curved-path SAR, geolocation error analysis, GeoSAR.

I. INTRODUCTION

Synthetic Aperture Radar (SAR) is a widely used microwave imaging device, which can get high resolution and high geolocation accuracy. Usually, the trajectory of airborne SAR or low-orbit SAR is a straight line, or after motion compensation, the linear part dominates. In these cases, the geolocation error can be modeled and analyzed by the uniform linear motion hypothesis, based on the range-Doppler (RD) equations [1], [2]. With the development of SAR technology, the carrying platforms, imaging modes and the applications of SAR are more and more diversified. In some occasions, such as the CSAR [3], GeoSAR [4], and missile-borne SAR [5], the trajectories cannot be equivalent to a uniform linear motion model, and the curve parts become more prominent. Therefore, the traditional geolocation error analysis based on linear model is not suitable, and the geolocation model for curved-path SAR should be studied.

So far, many papers for SAR imaging under curve trajectories have been published. In the case of constant acceleration, there have been many studies on the relationship between SAR imaging geometry and the influence of nonlinear phases [6], [7]. There have also been many advances in SAR frequency domain imaging algorithms under curved orbits. In [8], the two-dimensional spectrum of the echo under long-synthetic aperture time and large space variation is deduced, and the imaging focusing method is given. However, for the more general bending situation, the universal BP (Back Projection) algorithm may be more suitable for precisely focusing [9].

Other than imaging algorithms, there is less research on image geolocation and location error analysis under curve-path SAR. The usual way of positioning is to use the RD equations. When performing error analysis, much work is considered to add errors when using RD equations to further analyze the effects of these errors. In [10], SAR geolocation method is proposed using Range-Doppler (RD) equation. In [11], studies are done for GeoSAR based on RD equation. In these analysis, the Doppler centroid error is one of the error sources independent with the SAR velocity error and other errors. However, the Doppler centroid error is caused by factors such as velocity error and estimation methods, so it is not an essential error source. Moreover, these analyses do not combine the imaging process, but only assume the existence of errors when using the RD equation for positioning. So, the models in these works are implicit, which can't effectively guide the system design, error source budget, or the understanding of the SAR geolocation error.

In this paper, we derive a geolocation model for curved-path SAR with the generalized BP imaging algorithm.

The associate editor coordinating the review of this manuscript and approving it for publication was Dong Wang.

The corresponding model is given in both the spaceborne and airborne cases. The expressions of the relationship between the geolocation error and the error sources are explicit, which can be useful references for the error sources budget when designing the SAR system.

II. IMAGING GEOMETRY AND ERROR SETTING

Usually the trajectory of a curved-path SAR like the missile-borne SAR can be equivalent to a parabola, where the acceleration is constant. And in other curved-path SAR like the GeoSAR, the satellite trajectory in the synthetic aperture time can be fitted by polynomial, and the coefficients of the 4th or higher terms are very small compared with the low order term, which can be properly ignored. So, in this paper a third-ordered polynomial is used to approximate the SAR track. In practice, the higher-order terms can be fitted to requirements, and the processing methods are consistent. The imaging geometry of spaceborne SAR and airborne curved-path SAR is similar, but there are still some different places to note. We first establish the imaging geometry of the airborne curved-path SAR as shown in Fig. 1, then the geometry of the spaceborne curved-path SAR is shown as Fig. 2.

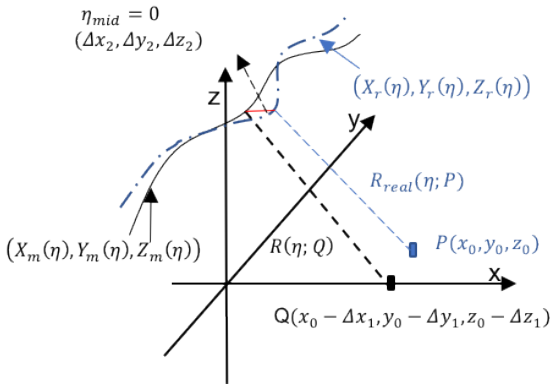

FIGURE 1. Imaging geometry of airborne SAR.

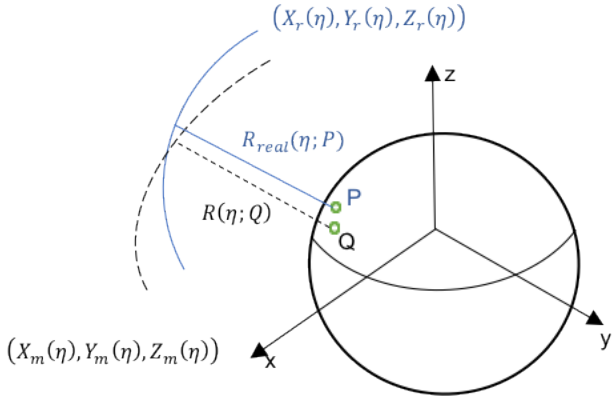

FIGURE 2. Imaging geometry of spaceborne SAR.

There are many error sources in the imaging geometry model, including, the velocity error and position error, the slant range error which caused by the system delay and the atmosphere, the height error of the scenario, the azimuth time error between pulse receiving and the trajectory measurements, etc. As in [12] and [13], the main errors are the velocity error, SAR position error, slant range error and the height error. Since the height error is not related to the SAR system, and the effects caused by height error is relatively simple, here we focus on the analysis model of the velocity error, the position error, and the slant range error, which is sufficient. Although the measurements of velocity and position have random errors in the actual system, when these measurements are used to obtain the SAR trajectory information, a fitting operation is performed. Moreover, the synthetic aperture time is usually not a long time, so the errors between the fitted trajectory and the real trajectory usually can be modeled by polynomial. Therefore, the position and velocity error modeled by polynomial can be quite general.

The following shows the geometric relationship of the imaging process and the corresponding error settings. Let the SAR trajectory equation be shown in (1).

$$\begin{cases} X_r(\eta) = p_x + (v_x + \Delta v_x)\eta + a_x\eta^2 + b_x\eta^3 \\ Y_r(\eta) = p_y + (v_y + \Delta v_y)\eta + a_y\eta^2 + b_y\eta^3 \\ Z_r(\eta) = p_z + (v_z + \Delta v_z)\eta + a_z\eta^2 + b_z\eta^3 \end{cases} \tag{1}$$

In the above equations, (X_r, Y_r, Z_r) is the instantaneous position of the SAR. Andη is the azimuth time. Set the center moment $\eta_{mid} = 0$. SAR position is (p_x, p_y, p_z) at this moment. The measured SAR trajectory will be biased due to the existence of measurement errors. Set the measured velocity error as $(-\Delta v_x, -\Delta v_y, -\Delta v_z)$, and the position of the SAR at the center moment is measured as (q_x, q_y, q_z). Therefore, the measured SAR trajectory can be written as (2). At this point we have considered the SAR trajectory error over the entire synthetic aperture time.

$$\begin{cases} X_m(\eta) = q_x + v_x\eta + a_x\eta^2 + b_x\eta^3 \\ Y_m(\eta) = q_y + v_y\eta + a_y\eta^2 + b_y\eta^3 \\ Z_m(\eta) = q_z + v_z\eta + a_z\eta^2 + b_z\eta^3 \end{cases} \tag{2}$$

The position of the target can be arbitrarily set to $P(x_0, y_0, z_0)$. Suppose the deviation between the target and the peak of imaging result is $(\Delta x_1, \Delta y_1, \Delta z_1)$, and the deviation between the real SAR position and measured SAR position at the center moment is $(\Delta x_2, \Delta y_2, \Delta z_2)$, shown as (3).

$$q_x = p_x + \Delta x_2, q_y = p_y + \Delta y_2, q_z = p_z + \Delta z_2 \tag{3}$$

The situation of spaceborne SAR is similar. Fig. 2 shows the geometric relationship in the case of spaceborne SAR. The above settings for SAR trajectories and errors still can be applied. However, it is worth noting that in the above settings, the target we set is stationary. In some coordinate systems, the target is moving as the Earth rotates. In order to follow the above settings, we need to choose the appropriate coordinate system. In this paper, the spaceborne SAR geolocation error model is derived in the WGS84 [14] coordinate system. Under this coordinate system, the target is stationary.

In the process of acquiring echoes, in addition to the above-mentioned error sources, there is an error in the slant range history due to errors such as delay errors in the echo acceptance process. Therefore, the true range history of the target deviates from the slant range history used in the imaging process. The relationship between actual range history $R_{real}(\eta)$ and the measured range history $R(\eta)$ is shown as (4), where ΔR is the deviation caused by the error sources other than the SAR trajectory errors such as the delay error. For convenience, in the subsequent derivation, ΔR is incorporated into the measured range history$R(\eta)$.

$$R_{real}(\eta) = R(\eta) + \Delta R \tag{4}$$

III. GEOLOCATION ERROR ANALYSIS

The model of error analysis in this paper is based on BP imaging algorithm. For the BP imaging algorithm, it sets a mesh grid in the imaging area. Then for each grid point, the matched filter is constructed according to the measured SAR trajectory, and the signals are filtered and accumulated along the calculated range migration curve. Because of the SAR trajectory error, there is a deviation between the distance data used for imaging and the true value. The actual range history can be written as (5). The SAR echo signal after range compression can be written as (6).

$$R_{real}(\eta; P) = \sqrt{(X_r(\eta)-x_0)^2+(Y_r(\eta)-y_0)^2+(Z_r(\eta)-z_0)^2} \tag{5}$$

$$\begin{aligned} s(t,\eta;P) = {} & rect\left(\frac{\eta}{T_{syn}}\right) \\ & \cdot sinc\left(t-\frac{2R_{real}(\eta;P)}{c}\right) \\ & \times \exp\left(-j\frac{4\pi}{\lambda}R_{real}(\eta;P)\right) \end{aligned} \tag{6}$$

where t is the range time, T_{syn} stands for the synthetic aperture time, λ is the wavelength of the carrier, c represents the speed of light. And *rect(x)* represents a rectangular window function. At a certain imaging grid point Q (x, y, z), matched function constructed by BP algorithm can be written as (7).

$$\begin{aligned} H_{BP}(t,\eta;x,y) = {} & rect\left(\frac{\eta}{T_{syn}}\right) sinc\left(t-\frac{2R(\eta;Q)}{c}\right) \\ & \times \exp\left(j\frac{4\pi}{\lambda}R(\eta;Q)\right) \end{aligned} \tag{7}$$

where range migration curve $R(\eta; Q)$ can be written as (8).

$$R(\eta;Q) = \sqrt{(X_m(\eta)-x)^2+(Y_m(\eta)-y)^2+(Z_m(\eta)-z)^2} + \Delta R \tag{8}$$

Due to the error sources, the above matched function does not match well with the echo signal when $x = x_0, y = y_0, z = z_0$. So, the energy cannot be well accumulated to the original position of the target. According to the above matched filter, the geolocation error we are looking for is just the deviation between the peak position of the energy accumulation and the original target position. Then in order to match the function with the echo signal, it should have the formula as (9).

$$R(\eta; x_0-\Delta x_1, y_0-\Delta y_1, z_0-\Delta z_1) \approx R_{real}(\eta; x_0, y_0, z_0) \tag{9}$$

After performing Taylor expansion of $R(\eta)$ at (x_0, y_0, z_0), and Taylor expansion of $R_{real}(\eta)$ at (v_x, v_y, v_z), the above formula will become clearer. Please note that the selection of variables has changed while performing Taylor expansion. Let's do some simplification first, Let:

$$\Delta x = \Delta x_1 + \Delta x_2, \Delta y = \Delta y_1 + \Delta y_2, \Delta z = \Delta z_1 + \Delta z_2 \tag{10}$$

Now, we combine the SAR position deviation at the center time with the deviation of the target point into a total deviation. Then we have the Taylor expansion shown as (11) and (12), first order term is retained.

$$\begin{aligned} & R(\eta) \\ & \approx R_c + \frac{(X'-x_0)\Delta x + (Y'-y_0)\Delta y + (Z'-z_0)\Delta z + \Delta R R_0}{R_c} \end{aligned} \tag{11}$$

$$\begin{aligned} & R_{real}(\eta) \\ & \approx R_c + \frac{(X'-x_0)\eta\Delta v_x + (Y'-y_0)\eta\Delta v_y + (Z'-z_0)\eta\Delta v_z}{R_c} \end{aligned} \tag{12}$$

where:

$$\begin{aligned} R_c &= \sqrt{(X'-x_0)^2+(Y'-y_0)^2+(Z'-z_0)^2} \\ X' &= p_x + v_x\eta + a_x\eta^2 + b_x\eta^3 \\ Y' &= p_y + v_y\eta + a_y\eta^2 + b_y\eta^3 \\ Z' &= p_z + v_z\eta + a_z\eta^2 + b_z\eta^3 \\ R_0 &= \sqrt{(p_x-x_0)^2+(p_y-y_0)^2+(p_z-z_0)^2} \end{aligned} \tag{13}$$

It can be seen that (11) and (12) are just different in numerators. In order to make $R(\eta)$ and $R_{real}(\eta)$ as equal as possible, the low-order terms that make up the main component should be consistent. In the continuous function space, due to the non-orthogonality of the Taylor expansion polynomial, using the Taylor polynomial to approximate the function, the high-order term coefficients decay slowly. At the same time, the high-order items still contain components related to the first-order items, and therefore also affect the location error. Orthogonal Legendre orthogonal polynomials obtained by orthogonalization of Taylor polynomials can better approximate the continuous function [15]. Meanwhile, it also helps us to consider the influence of the high order term coefficients of the trajectory. The specific operation is as follows. Let:

$$\begin{aligned} f(\eta) &= (X'-x_0)\eta\Delta v_x + (Y'-y_0)\eta\Delta v_y + (Z'-z_0)\eta\Delta v_z \\ &= A_1\xi + A_2\xi^2 + A_3\xi^3 + A_4\xi^4 \end{aligned}$$

$$= \left(\frac{1}{3}A_2 + \frac{1}{5}A_4\right) P_0(\xi) + \left(A_1 + \frac{3}{5}A_3\right) P_1(\xi) + \left(\frac{2}{3}A_2 + \frac{4}{7}A_4\right) P_2(\xi) + \frac{2}{5}A_3 P_3(\xi) + \frac{8}{35}A_4 P_4(\xi) \tag{14}$$

where $\xi = \frac{2\eta}{T_{syn}}$, $-1 \ll \xi \ll 1$. $P_0(\xi), P_1(\xi), \ldots\ldots$ is the Legendre polynomial. Let $T = T_{syn}/2$, the coefficient is as follows:

$$\begin{aligned} A_1 &= (p_x \Delta v_x - x_0 \Delta v_x + p_y \Delta v_y - y_0 \Delta v_y + p_z \Delta v_z - z_0 \Delta v_z) T \\ A_2 &= (v_x \Delta v_x + v_y \Delta v_y + v_z \Delta v_z) T^2 \\ A_3 &= (a_x \Delta v_x + a_y \Delta v_y + a_z \Delta v_z) T^3 \\ A_4 &= (b_x \Delta v_x + b_y \Delta v_y + b_z \Delta v_z) T^4 \end{aligned} \tag{15}$$

Since R_c is also a function of η, some simplifications need to be made as follows:

$$R_c \approx R_0 + \frac{(p_x - x_0) v_x + (p_y - y_0) v_y + (p_z - z_0) v_z}{R_0} \eta \tag{16}$$

The above equation shows that the slant range error introduces a linear part in the slant range expression numerator. If the slant range error is large, the above equation can be expanded to higher order terms to improve accuracy. Constant terms can be retained to meet less high precision requirements. Therefore, like (14), we can get:

$$\begin{aligned} g(\eta) &= (X' - x_0) \Delta x + (Y' - y_0) \Delta y + (Z' - z_0) \Delta z + \Delta R R_0 \\ &= B_0 + B_1 \xi + B_2 \xi^2 + B_3 \xi^3 \\ &= \left(B_0 + \frac{1}{3}B_2\right) P_0(\xi) + \left(B_1 + \frac{3}{5}B_3\right) P_1(\xi) + \frac{2}{3}B_2 P_2(\xi) + \frac{2}{5}B_3 P_3(\xi) \end{aligned} \tag{17}$$

The coefficient is as follows:

$$\begin{aligned} B_0 &= p_x \Delta x - x_0 \Delta x + p_y \Delta y - y_0 \Delta y + p_z \Delta z - z_0 \Delta z + \Delta R R_0 \\ B_1 &= (v_x \Delta x + v_y \Delta y + v_z \Delta z) T \\ B_2 &= (a_x \Delta x + a_y \Delta y + a_z \Delta z) T^2 \\ B_3 &= (b_x \Delta x + b_y \Delta y + b_z \Delta z) T^3 \end{aligned} \tag{18}$$

In order to solve the geolocation error, we need to get three equations. To begin with, we should consider the constraints of the imaging plane, the imaging peak point must be on the imaging plane. Secondly, according to the above two expansion equations, the constant term and the first term of the two are respectively equalized to obtain two equations. The equations are shown as (19). Regarding the first equation, the situation of spaceborne SAR and airborne SAR is not the same. We will discuss it separately below.

$$\begin{cases} h(x_0 - \Delta x_1, y_0 - \Delta y_1, z_0 - \Delta z_1) = 0 \\ \frac{1}{3}A_2 + \frac{1}{5}A_4 = B_0 + \frac{1}{3}B_2 \\ A_1 + \frac{3}{5}A_3 = B_1 + \frac{3}{5}B_3 \end{cases} \tag{19}$$

A. AIRBORNE SAR

In the geometric relationship shown in Figure 1, the ground is our imaging plane. According to this we can get the specific form of the first equation. The equations are relisted as (20), where h is the elevation information of the imaging plane.

$$\begin{cases} z_0 - \Delta z_1 = h \\ \frac{1}{3}A_2 + \frac{1}{5}A_4 = B_0 + \frac{1}{3}B_2 \\ A_1 + \frac{3}{5}A_3 = B_1 + \frac{3}{5}B_3 \end{cases} \tag{20}$$

Note that $(\Delta x_2, \Delta y_2, \Delta z_2)$ is the measured deviation of the SAR trajectory at the center time and are known amounts. The three unknowns that need to be solved are the target location deviations $(\Delta x_1, \Delta y_1, \Delta z_1)$. In (10), we combine the two deviations into one, so we first solve for $(\Delta x, \Delta y, \Delta z)$ and then get the value of $(\Delta x_1, \Delta y_1, \Delta z_1)$ according to (10). Without loss of generality, we can assume that both the position error of the SAR at the center time and the elevation of the target are zero. Then we only need to solve $(\Delta x, \Delta y, \Delta z)$. By solving the above equations and performing an appropriate arrangement, we can get the following expression of Δx:

$$\Delta x = \lambda_1 \Delta v_x + \lambda_2 \Delta v_y + \lambda_3 \Delta v_z + \lambda_4 \Delta R \tag{21}$$

where the coefficients are:

$$\begin{aligned} \lambda_1 &= (p_x - x)\theta_1 T + \theta_2 v_x T^2 + \theta_3 a_x T^3 + \theta_4 b_x T^4 \\ \lambda_2 &= (p_y - y)\theta_1 T + \theta_2 v_y T^2 + \theta_3 a_y T^3 + \theta_4 b_y T^4 \\ \lambda_3 &= (p_z - y)\theta_1 T + \theta_2 v_z T^2 + \theta_3 a_z T^3 + \theta_4 b_z T^4 \\ \lambda_4 &= h_{yb} R_c \left(h_{xb} e_{ya} - h_{yb} e_{xa}\right)^{-1} \end{aligned} \tag{22}$$

Further, the second set of parameters is as follows:

$$\begin{aligned} \theta_1 &= e_{ya} \left(h_{xb} e_{ya} - h_{yb} e_{xa}\right)^{-1} \\ \theta_2 &= -h_{yb} \left(3h_{xb} e_{ya} - 3h_{yb} e_{xa}\right)^{-1} \\ \theta_3 &= 3e_{ya} \left(5h_{xb} e_{ya} - 5h_{yb} e_{xa}\right)^{-1} \\ \theta_4 &= -h_{yb} \left(5h_{xb} e_{ya} - 5h_{yb} e_{xa}\right)^{-1} \end{aligned} \tag{23}$$

The last set of parameters is as follows:

$$\begin{aligned} e_{xa} &= p_x - x_0 + \frac{1}{3}a_x T^2 \\ e_{ya} &= p_y - y_0 + \frac{1}{3}a_y T^2 \\ h_{xb} &= v_x T + 3b_x T^3/5 \\ h_{yb} &= v_y T + 3b_y T^3/5 \end{aligned} \tag{24}$$

The expression of Δy is similar:

$$\Delta y = \mu_1 \Delta v_x + \mu_2 \Delta v_y + \mu_3 \Delta v_z + \mu_4 \Delta R \tag{25}$$

Parameters are as follows:

$$\begin{aligned}\mu_1 &= (p_x - x_0)\,\omega_1 T + \omega_2 v_x T^2 + \omega_3 a_x T^3 + \omega_4 b_x T^4\\ \mu_2 &= \left(p_y - y_0\right)\omega_1 T + \omega_2 v_y T^2 + \omega_3 a_y T^3 + \omega_4 b_y T^4\\ \mu_3 &= (p_z - z_0)\,\omega_1 T + \omega_2 v_z T^2 + \omega_3 a_z T^3 + \omega_4 b_z T^4\\ \mu_4 &= -(R_c + e_{xa}\lambda_4)/e_{ya}\end{aligned} \tag{26}$$

The second set of parameters is as follows:

$$\begin{aligned}\omega_1 &= -\frac{e_{xa}}{e_{ya}}\theta_1,\ \omega_2 = \frac{1}{3e_{ya}} - \frac{e_{xa}}{e_{ya}}\theta_2\\ \omega_3 &= -\frac{e_{xa}}{e_{ya}}\theta_3,\ \omega_4 = \frac{1}{5e_{ya}} - \frac{e_{xa}}{e_{ya}}\theta_4\end{aligned} \tag{27}$$

Suppose the numerators are not equal to zero. Otherwise, the location error can be solved directly in this constraint. It can be seen that the expression of the geolocation error is the weighted sum of the error sources. The proportion of each kind of error is very clear.

Simplistically, if the coefficients of the orbit high-order terms are 0, then the position deviation can be expressed as (28), shown at the top of the next page. Location deviation can still be regarded as a weighted sum of the error sources, the form is more simple and direct.

Again, suppose the numerator is not equal to zero. Otherwise, the target point becomes the projection of the SAR on the ground at the center of time, which is impossible. This is the positioning situation under the traditional model. The traditional model uses the motion compensation or other means to make the trajectory equivalent to a straight line near the imaging center moment, and then uses the RD equation for positioning. However, this traditional model does not apply to the case where the SAR trajectory is highly curved. It will be verified in subsequent sections. To make the results more intuitive, we set that the velocity direction of the SAR is along the y direction and, at the central moment, the coordinates of the SAR are $(0, 0, p_z)$, and the coordinates of the target are $(x_0, y_0, 0)$. Results are shown as (29).

$$\begin{aligned}\Delta x &= (x_0 y_0 \Delta v_x + y_0^2 \Delta v_y - y_0 p_z \Delta v_z + v_y R_0 \Delta R)/(x_0 v_y - v_x y_0)\\ \Delta y &= (x_0^2 \Delta v_x + x_0 y_0 \Delta v_y - x_0 p_z \Delta v_z + v_x R_0 \Delta R)/(v_x y_0 - x_0 v_y)\end{aligned} \tag{29}$$

Here, if y_0 is equal to 0, it means that there is no squint angle. Then it can be seen from (29) that the geolocation error in the y direction, or azimuth direction, is not affected by the velocity error in the y direction without the squint angle or velocity errors in other directions and the geolocation error in the x direction, or range direction, is only affected by the slant range error. Further, if the value of y_0 is relatively large, the location error is also large. In other words, under the traditional model, the larger the squint angle, the greater the influence on the geolocation error.

Under the curve model, we set that at the center moment, the SAR velocity direction is along the y direction, and the position coordinate value in the y direction is 0. Then this brings that the larger the value of y_0, the larger squint angle at the center moment. Resolve the above equations and write the solution as a functional form about y_0 as (30), where k,c_i are the coefficients, and their expression is not given. Due to the curved trajectory, the angle between the target and the beam direction of the antenna varies greatly during the synthetic aperture time. Therefore, the relationship between squint angle and geolocation error is not as obvious as that under the traditional model. However, if the parameters are given, the influence of the different squint angles on the geolocation error can be analyzed according to (30).

$$\begin{aligned}\Delta y &= c_2/(y_0 + c_1) + c_3\\ \Delta x &= k y_0 + c_4/(y_0 + c_1) + c_5\end{aligned} \tag{30}$$

B. SPACEBORNE SAR

In the geometric relationship shown in Figure 2, the Earth's surface is our imaging plane, so the target and imaging peak point should be on this surface. Taking altitude information of the target point into account, the new equations are obtained as follows

$$\begin{cases}\dfrac{1}{3}A_2 + \dfrac{1}{5}A_4 = B_0 + \dfrac{1}{3}B_2\\ A_1 + \dfrac{3}{5}A_3 = B_1 + \dfrac{3}{5}B_3\\ \dfrac{(x_0 - \Delta x_1)^2 + (y_0 - \Delta y_1)^2}{(R_E + h)} + \dfrac{(z_0 - \Delta z_1)^2}{(R_P + h)} = 1\end{cases} \tag{31}$$

where R_E is the equatorial radius of the Earth and R_P is the polar radius of the Earth, h stands for the altitude of the target. Solving this set of equations gives an expression for the location error, but since the Earth equation is a quadratic equation, the results may not be intuitive. Let's do some simplification. Because the Earth approximates a sphere with a large radius, we can assume that the imaging plane is a tangent plane through the target point. Then the imaging peak point and the target point are both on this tangent plane. When the earth is regarded as a sphere, the position vector of the target just follows the normal direction of the tangent plane through the target point. According to the geometric relationship, the location error vector is perpendicular to the target position vector. Then we can get the new equations as follows:

$$\begin{cases}\dfrac{1}{3}A_2 + \dfrac{1}{5}A_4 = B_0 + \dfrac{1}{3}B_2\\ A_1 + \dfrac{3}{5}A_3 = B_1 + \dfrac{3}{5}B_3\\ x_0\Delta x_1 + y_0\Delta y_1 + z_0\Delta z_1 = 0\end{cases} \tag{32}$$

By solving the above equations and performing an appropriate arrangement, we can get the following expression of Δy_1:

$$\begin{aligned}\Delta y_1 = {} & \rho_1\Delta v_x + \rho_2\Delta v_y + \rho_3\Delta v_z + \rho_4\Delta x_2\\ & + \rho_5\Delta y_2 + \rho_6\Delta z_2 + \rho_7\Delta R\end{aligned} \tag{33}$$

where the coefficients are:

$$\begin{aligned}\rho_1 &= (p_x - x_0)\,\theta_1 T + \theta_2 v_x T^2 + \theta_3 a_x T^3 + \theta_4 b_x T^4\\ \rho_2 &= \left(p_y - y_0\right)\theta_1 T + \theta_2 v_y T^2 + \theta_3 a_y T^3 + \theta_4 b_y T^4\end{aligned}$$

$$\Delta x = \frac{(p_y - y_0)(p_x - x_0)\Delta v_x + (p_y - y_0)^2 \Delta v_y + (p_y - y_0)(p_z - z_0)\Delta v_z + v_y R_0 \Delta R}{(p_y - y_0) v_x - (p_x - x_0) v_y}$$
$$\Delta y = \frac{(p_x - x_0)^2 \Delta v_x + (p_x - x_0)(p_y - y_0)\Delta v_y + (p_x - x_0)(p_z - z_0)\Delta v_z + v_x R_0 \Delta R}{(p_x - x_0) v_y - (p_y - y_0) v_x} \quad (28)$$

$$\begin{aligned}
\rho_3 &= (p_z - z_0)\theta_1 T + \theta_2 v_z T^2 + \theta_3 a_z T^3 + \theta_4 b_z T^4 \\
\rho_4 &= \theta_1 v_x T - \left(3(p_x - x_0) + a_x T^2\right)\theta_2 + \theta_3 b_x T^3 \\
\rho_5 &= \theta_1 v_y T - \left(3(p_y - y_0) + a_y T^2\right)\theta_2 + \theta_3 b_y T^3 \\
\rho_6 &= \theta_1 v_z T - \left(3(p_z - z_0) + a_z T^2\right)\theta_2 + \theta_3 b_z T^3 \\
\rho_7 &= -15R_c / \left(n_y l_{yz} - n_x l_{yz}\right)
\end{aligned} \quad (34)$$

The second set of parameters is as follows:

$$\begin{aligned}
\theta_1 &= -5n_x / \left(n_y l_{yz} - n_x l_{yz}\right) \\
\theta_2 &= 5 / \left(n_y l_{yz} - n_x l_{yz}\right) \\
\theta_3 &= -3n_x / \left(n_y l_{yz} - n_x l_{yz}\right) \\
\theta_4 &= 3 / \left(n_y l_{yz} - n_x l_{yz}\right)
\end{aligned} \quad (35)$$

The last set of parameters is as follows:

$$\begin{aligned}
n_x &= (15(p_x - x_0) + 5a_x T^2)/l_{xz} \\
&\quad - (15(p_z - z_0) + 5a_z T^2)x_0/(z_0 l_{xz}) \\
n_y &= (15(p_y - y_0) + 5a_y T^2)/l_{yz} \\
&\quad - (15(p_z - z_0) + 5a_z T^2)y_0/(z_0 l_{yz}) \\
l_{xz} &= \left(5v_x T + 3b_x T^3\right) - (5v_z T + 3b_z T^3)x_0/z_0 \\
l_{yz} &= \left(5v_y T + 3b_y T^3\right) - (5v_z T + 3b_z T^3)y_0/z_0
\end{aligned} \quad (36)$$

The expression of Δx_1 is similar:

$$\begin{aligned}
\Delta x_1 &= \gamma_1 \Delta v_x + \gamma_2 \Delta v_y + \gamma_3 \Delta v_z + \gamma_4 \Delta x_2 \\
&\quad + \gamma_5 \Delta y_2 + \gamma_6 \Delta z_2 + \gamma_7 \Delta R
\end{aligned} \quad (37)$$

where the coefficients are:

$$\begin{aligned}
\gamma_1 &= (p_x - x_0)\omega_1 T + \omega_2 v_x T^2 + \omega_3 a_x T^3 + \omega_4 b_x T^4 \\
\gamma_2 &= (p_y - y_0)\omega_1 T + \omega_2 v_y T^2 + \omega_3 a_y T^3 + \omega_4 b_y T^4 \\
\gamma_3 &= (p_z - z_0)\omega_1 T + \omega_2 v_z T^2 + \omega_3 a_z T^3 + \omega_4 b_z T^4 \\
\gamma_4 &= (p_x - x_0)\omega_5 + \omega_6 v_x T + \omega_7 a_x T^2 + \omega_8 b_x T^3 \\
\gamma_5 &= (p_y - y_0)\omega_5 + \omega_6 v_y T + \omega_7 a_y T^2 + \omega_8 b_y T^3 \\
\gamma_6 &= (p_z - z_0)\omega_5 + \omega_6 v_z T + \omega_7 a_z T^2 + \omega_8 b_z T^3 \\
\gamma_7 &= -l_{yz}\rho_7 / l_{xz}
\end{aligned} \quad (38)$$

The second set of parameters is as follows:

$$\begin{aligned}
\omega_1 &= \left(5 - l_{yz}\theta_1\right)/l_{xz},\ \omega_5 = 3\theta_2 l_{yz}/l_{xz} \\
\omega_2 &= -l_{yz}\theta_2/l_{xz},\ \omega_6 = \left(5 - \theta_1 l_{yz}\right)/l_{xz} \\
\omega_3 &= (3 - l_{yz}\theta_3)/l_{xz},\ \omega_7 = \theta_2 l_{yz}/l_{xz} \\
\omega_4 &= -l_{yz}\theta_4/l_{xz},\ \omega_8 = \left(3 - \theta_3 l_{yz}\right)/l_{xz}
\end{aligned} \quad (39)$$

Finally, we can get the expression of Δz_1:

$$\begin{aligned}
\Delta z_1 &= \delta_1 \Delta v_x + \delta_2 \Delta v_y + \delta_3 \Delta v_z + \delta_4 \Delta x_2 \\
&\quad + \delta_5 \Delta y_2 + \delta_6 \Delta z_2 + \delta_7 \Delta R
\end{aligned} \quad (40)$$

where the coefficients are:

$$\begin{aligned}
\delta_1 &= (p_x - x_0)\varphi_1 T + \varphi_2 v_x T^2 + \varphi_3 a_x T^3 + \varphi_4 b_x T^4 \\
\delta_2 &= (p_y - y_0)\varphi_1 T + \varphi_2 v_y T^2 + \varphi_3 a_y T^3 + \varphi_4 b_y T^4 \\
\delta_3 &= (p_z - z_0)\varphi_1 T + \varphi_2 v_z T^2 + \varphi_3 a_z T^3 + \varphi_4 b_z T^4 \\
\delta_4 &= (p_x - x_0)\varphi_5 + \varphi_6 v_x T + \varphi_7 a_x T^2 + \varphi_8 b_x T^3 \\
\delta_5 &= (p_y - y_0)\varphi_5 + \varphi_6 v_y T + \varphi_7 a_y T^2 + \varphi_8 b_y T^3 \\
\delta_6 &= (p_z - z_0)\varphi_5 + \varphi_6 v_z T + \varphi_7 a_z T^2 + \varphi_8 b_z T^3 \\
\delta_7 &= -(x_0\gamma_7 + y_0\rho_7)/z_0
\end{aligned} \quad (41)$$

The second set of parameters is shown as:

$$\begin{aligned}
\varphi_1 &= -(x_0\omega_1 + y_0\theta_1)/z_0,\ \varphi_5 = -(x_0\omega_5 - 3y_0\theta_2)/z_0 \\
\varphi_2 &= -(x_0\omega_2 + y_0\theta_2)/z_0,\ \varphi_6 = -(x_0\omega_6 + y_0\theta_1)/z_0 \\
\varphi_3 &= -(x_0\omega_3 + y_0\theta_3)/z_0,\ \varphi_7 = -(x_0\omega_7 - y_0\theta_2)/z_0 \\
\varphi_4 &= -(x_0\omega_4 + y_0\theta_4)/z_0,\ \varphi_6 = -(x_0\omega_8 + y_0\theta_3)/z_0
\end{aligned} \quad (42)$$

The expression of the solution of the above equations is relisted as:

$$\begin{cases}
\Delta x_1 = \boldsymbol{\gamma}_v^{\mathrm{T}} \boldsymbol{\Delta v} + \boldsymbol{\gamma}_q^{\mathrm{T}} \boldsymbol{\Delta q} + \gamma_7 \Delta R \\
\Delta y_1 = \boldsymbol{\rho}_v^{\mathrm{T}} \boldsymbol{\Delta v} + \boldsymbol{\rho}_q^{\mathrm{T}} \boldsymbol{\Delta q} + \rho_7 \Delta R \\
\Delta z_1 = \boldsymbol{\delta}_v^{\mathrm{T}} \boldsymbol{\Delta v} + \boldsymbol{\delta}_q^{\mathrm{T}} \boldsymbol{\Delta q} + \delta_7 \Delta R
\end{cases} \quad (43)$$

where $\boldsymbol{\Delta v} = (\Delta v_z, \Delta v_y, \Delta v_z)^T$, $\boldsymbol{\Delta q} = (\Delta x_2, \Delta y_2, \Delta z_2)^T$, and the coefficient vectors are:

$$\begin{aligned}
\boldsymbol{\gamma_v} &= (\gamma_1, \gamma_2, \gamma_3)^T, \quad \boldsymbol{\gamma_q} = (\gamma_4, \gamma_5, \gamma_6)^T \\
\boldsymbol{\rho_v} &= (\rho_1, \rho_2, \rho_3)^T, \quad \boldsymbol{\rho_q} = (\rho_4, \rho_5, \rho_6)^T \\
\boldsymbol{\delta_v} &= (\delta_1, \delta_2, \delta_3)^T, \quad \boldsymbol{\delta_q} = (\delta_4, \delta_5, \delta_6)^T
\end{aligned} \quad (44)$$

The form of the solution is still the weighted sum of each error source. The effect of each error source on the final location deviation is visually visible. Until now, we have obtained the theoretical models of geolocation error in both spaceborne SAR and airborne SAR.

IV. SIMULATION AND ANALYSIS

It is better to use actual data. However, as for the actual data, the measure error for the trajectory is unknown. Although we can add errors to the measured trajectory of real data, and take the measure one as the real one (without error), it cannot

TABLE 1. Main simulation parameters of airborne SAR.

PARAMETERS	VALUE1	VALUE2
Carrier frequency	2GHz	4Ghz
Chirp bandwith	20MHZ	20MHZ
Chirp duration	10μs	10μs
Pulse repetition frequency	100Hz	185Hz
Platform velocity	(10,200,10)m/s	(0,600,0)m/s
Acceleration	(20,10,-15)m/s^2	(0,7,-9)m/s^2
Secondary acceleration	(-10,15,10)m/s^3	(0,2,-1)m/s^3
SAR position at center time	(0,0,100)km	(0,0,300)km
Squint angle	20°	20°
Look angle	45°	45°
Target position	(100,51.47,0)km	(357.5,169.9,0)km
Grid interval	3.5m	2.5m

verity the model precisely. Here we use simulation data to verify it. Because the errors in simulations are known and can be controlled, the verification work can be done effectively. Similarly, we start with the airborne SAR.

A. AIRBORNE SAR SIMULATION

We verify the correctness of the model by simulating two sets of parameters. The first set of parameters is the case where the track has a large degree of bending. The second group simulates the situation of missile-borne SAR. Unlike the case where constant acceleration is generally considered, the influence of secondary acceleration is appropriately considered. We compare the simulation results with the traditional model and the curve model proposed in this paper. The results demonstrate the validity of the curve model. The main parameters are as follows.

In the simulation experiment, the specific geolocation deviation results are given for the Value1, and the comparison between the model and the simulation results is given for the Value2. During the simulation process, the peak value was searched after the imaging result was interpolated 64 times. The simulation results are shown in Fig. 3-6. From the simulation results of the two sets of simulation parameters, it can be seen that with the variation of the error sources, the traditional model and the simulation results are greatly different, but the curve model is very consistent with the simulation results, which proves the effectiveness of the curve model relative to the traditional model. For the second group of approximate parabolic models, the coefficients of the higher order terms are not very large, and the synthetic aperture time is not long, so that the traditional model can basically keep up with the

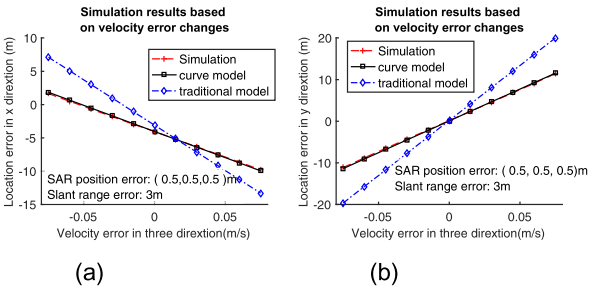

FIGURE 3. Simulation results of value 1 based on velocity error changes. (a) Location error in x direction. (b) Location error in y direction.

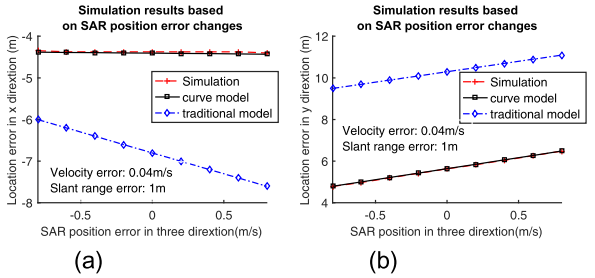

FIGURE 4. Simulation results of value 1 based on SAR position error changes. (a) Location error in x direction. (b) Location error in y direction.

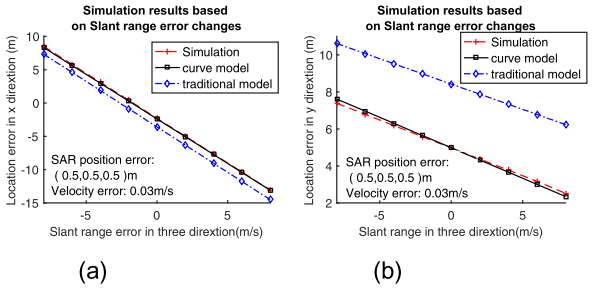

FIGURE 5. Simulation results of value 1 based on slant range error changes. (a) Location error in x direction. (b) Location error in y direction.

error trend, but it is still not as good as the curve model. The imaging result of the interpolated target point is also given. Compared with the case without errors, the addition of the errors do not cause significant defocus, meaning that the peak position can correspond to the target point. Two sets of simulation experiments have proved the effectiveness of the proposed model in the orbit of arbitrary bending degree.

B. SPACEBORNE SAR SIMULATION

We will next carry out a series of slightly complex spaceborne SAR simulations. Again, the SAR orbit error setting is done in the WGS84 coordinate system, that is, according to our theoretical model, we must set it in the coordinate system where the target does not move. Medium and high orbital simulations are performed separately. Simulation parameters are derived from actual spaceborne SAR parameters, and the main simulation parameters are as follows:

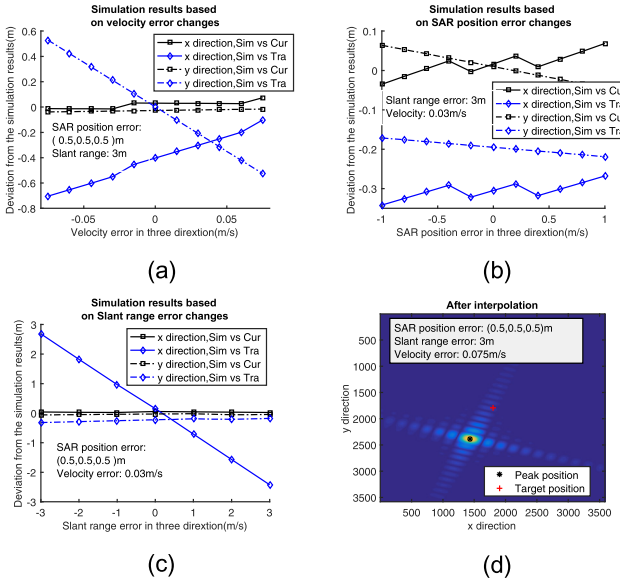

FIGURE 6. Simulation results of value 2. (a) Deviation between simulation and models based on velocity error changes. (b) Deviation between simulation and models based on SAR position error changes. (c) Deviation between simulation and models based on slant range changes. Sim stands for the simulation, Cur stands for the curve model and Tra stands for the traditional model.

TABLE 2. Main simulation parameters of spaceborne SAR.

PARAMETERS	MEDIUM ORBIT	HIGH ORBIT
Carrier frequency	5.4GHz	1.25Ghz
Chirp bandwith	30MHZ	160MHZ
Chirp duration	$10\mu s$	$10\mu s$
Pulse repetition frequency	1300Hz	150Hz
Azimuth antenna size	5.4m	22m
Incident angle	41.65°	29.6°
Squint angle	$16.35°$	7.70°
Orbit hight	7737km	35793km
Longitude of the ascending node	$60°$	$88°$
Orbital inclination	16°	16°
Argumen of perigee	$90°$	$90°$
Target point latitude and longitude	$(109.47°N, 13.87°S)$	$(79.97°N, 12.97°S)$
Grid interval	3.5m	10m

Similarly, we observed the geolocation deviation by changing the velocity errors in three directions, and the velocity error settings in the three directions were the same. The peak value was searched after the imaging result was interpolated 64 times. The simulation results are shown in Fig. 7-9. In the

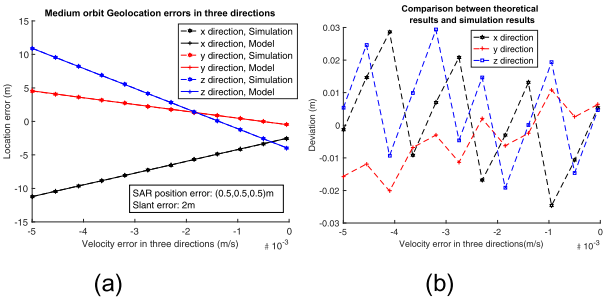

FIGURE 7. Simulation results of medium orbit SAR 2. (a) Geolocation errors in three directions. (b) Difference between simulation results and theoretical results.

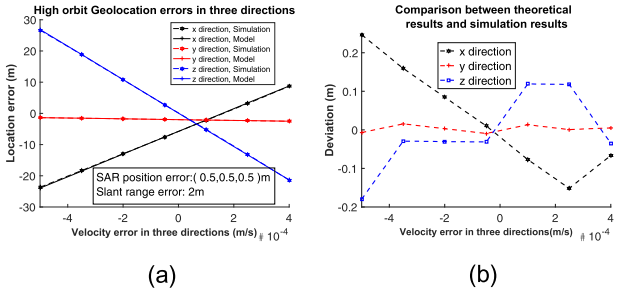

FIGURE 8. Simulation results of high orbit SAR. (a) Geolocation errors in three directions. (b) Difference between simulation results and theoretical results.

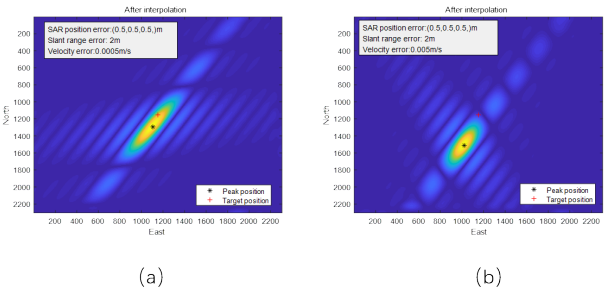

FIGURE 9. Simulation results after interpolation. (a) High orbit. (b) Medium orbit.

case of medium or high orbits, our models are in good agreement with the simulation results. The simulation results vary linearly, which is also consistent with the linear form of (43). Moreover, comparing the horizontal axes of Fig. 7 and Fig. 8, it can be found that the velocity errors of the high orbit are much smaller. However, observing their ordinates, geolocation errors are greater in the case of high orbit. From this it can be inferred that high orbits are more sensitive to speed errors. The imaging result of the interpolated target point is also given as Fig.8. In general, our model can accurately give the geolocation error.

V. CONCLUSIONS

In this paper, the geolocation error model of curved-path SAR based on BP imaging algorithm is proposed in airborne SAR and spaceborne SAR. The model we established is explicit,

and it reveals the relationship between SAR image geolocation error and the error sources. The results of simulations well confirm the correctness of theoretical analysis. Some conclusions similar to those in the case of using the frequency domain imaging algorithm are also verified. For instance, when the slant angle is larger, the geolocation error is more affected by measurement errors such as velocity; the higher the orbit height, the greater the influence of the velocity error on the location error. Geolocation error analysis based on BP algorithm in this paper is believed to provide an effective reference for the error source budget of curved-path SAR systems, such as GeoSAR, missile-borne SAR, etc.

REFERENCES

[1] M. Eineder, C. Minet, X. Cong, T. Fritz, and P. Steigenberger, "Towards imaging geodesy—Achieving centimetre pixel localization accuracy with TerraSAR-X," in *Proc. 8th Eur. Conf. Synth. Aperture Radar (VDE)*, Jun. 2010, pp. 1–4.

[2] J. Liu, X. Qiu, B. Han, and D. Xiao, "Study on geo-location of sliding spotlight mode of GF-3 satellite," in *Proc. IEEE 5th Asia–Pacific Conf. Synth. Aperture Radar (APSAR)*, Sep. 2015, pp. 417–420.

[3] W. Shen, Y. Lin, Y. Zhao, L. Yu, and W. Hong, "Initial result of single channel CSAR GMTI based on background subtraction," in *Proc. IEEE Int. Geosci. Remote Sens. Symp. (IGARSS)*, Jul. 2017, pp. 976–979.

[4] D. Bruno, S. E. Hobbs, and G. Ottavianelli, "Geosynchronous synthetic aperture radar: Concept design, properties and possible applications," *Acta Astronautica*, vol. 59, nos. 1–5, pp. 149–156, Jul./Sep. 2006.

[5] A. M. Cai, G. M. Yu, T. Y. Zheng, Z. G. Qi, and F. S. Huang, "The development trend and key technologies of missile-borne SAR," *Aerodyn. Missile J.*, no. 9, pp. 69–72, 2013.

[6] S. R. J. Axelsson, "Mapping performance of curved-path SAR," *IEEE Trans. Geosci. Remote Sens.*, vol. 40, no. 10, pp. 2224–2228, Oct. 2002.

[7] Y. Liao, S. Zhou, and L. Yang, "Focusing of SAR with curved trajectory based on improved hyperbolic range equation," *IEEE Geosci. Remote Sens. Lett.*, vol. 15, no. 3, pp. 454–458, Mar. 2018.

[8] S. Tang, C. Lin, Y. Zhou, H. C. So, L. Zhang, and Z. Liu, "Processing of long integration time spaceborne SAR data with curved orbit," *IEEE Trans. Geosci. Remote Sens.*, vol. 56, no. 2, pp. 888–904, Feb. 2018.

[9] A. F. Yegulalp, "Fast backprojection algorithm for synthetic aperture radar," in *Proc. IEEE Radar Conf. Radar Next Millennium*, Apr. 1999, pp. 60–65.

[10] J. C. Curlander and R. N. Mcdonough, *Synthetic Aperture Radar: Systems and Signal Processing*. Hoboken, NJ, USA: Wiley, 1991, pp. 3–7.

[11] T. Zeng, W. Yin, Z. Ding, and T. Long, "Geo-location error analysis in geosynchronous SAR," *Electron. Lett.*, vol. 50, no. 23, pp. 1741–1743, Nov. 2014.

[12] X. Cong, U. Balss, M. Eineder, and T. Fritz, "Imaging geodesy—Centimeter-level ranging accuracy with TerraSAR-X: An update," *IEEE Geosci. Remote Sens. Lett.*, vol. 9, no. 5, pp. 948–952, Sep. 2012.

[13] J. Liu, B. Han, C. Ding, D. Meng, and F. Li, "The preliminary results about positioning accuracy of GF-3 SAR satellite system," in *Proc. IEEE Int. Geosci. Remote Sens. Symp.*, Jul. 2017, pp. 6087–6089.

[14] Wikipedia. *World Geodetics System*. [Online]. Available: https://en.wikipedia.org/wiki/World_Geodetic_System

[15] B. D. Reddy, *Introductory Functional Analysis*. Hoboken, NJ, USA: Wiley, 1978.

[16] J. C. Curlander, "Location of spaceborne SAR imagery," *IEEE Trans. Geosci. Remote Sens.*, vol. GE-20, no. 3, pp. 359–364, Jul. 1982.

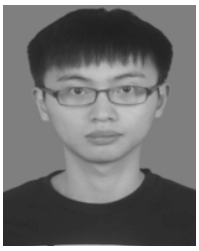

JUNBIN LIU received the B.S. degree in signal and information processing engineering from the South China University of Technology, Guangzhou, China, in 2017. He is currently pursuing the M.S. degree with the University of Chinese Academy of Sciences, also with the Key Laboratory of Technology in Geo-Spatial Information Processing and Application System, CAS, and also with the Institute of Electronics, Chinese Academy of Sciences. His research interests include synthetic aperture radar (SAR) signal processing and SAR calibration.

XIAOLAN QIU received the B.S. degree in electronic engineering from the University of Science and Technology of China, Hefei, China, in 2004, and the Ph.D. degree in signal and information processing from the Graduate University of the Chinese Academy of Sciences, Beijing, China, in 2009. She is currently with the Key Laboratory of Technology in Geo-Spatial Information Processing and Application System and also with the Institute of Electronics, Chinese Academy of Sciences, Beijing.

LIJIA HUANG received the B.S. degree in electronic engineering from Beihang University, Beijing, China, in 2006, and the Ph.D. degree in signal and information processing from the Graduate University of the Chinese Academy of Sciences, Beijing, China, in 2011. She is currently with the Key Laboratory of Technology in Geo-Spatial Information Processing and Application System, and also with the Institute of Electronics, Chinese Academy of Sciences, Beijing.

CHIBIAO DING received the B.S. and Ph.D. degrees in electronic engineering from Beihang University, Beijing, China, in 1997.

Since 1997, he has been with the Institute of Electronics, Chinese Academy of Sciences, Beijing, where he is currently a Research Fellow and the Vice Director. His main research interests include advanced SAR systems, signal processing technology, and information systems.